Full title: A VHL-1/HIF-1/SQRD1/COL-88 axis links extracellular matrix formation with longevity in *Caenorhabditis elegans*

Short title: VHL/HIF-1/SQRD1/COL-88 in extracellular matrix and longevity

Author list:

Willian Salgueiro[1,2,*], Reza Esmaillie[1,2,*], Katrin Bohl[1,2], Cyril Statzer[3], Puneet Bharill[1,2], Sebastian Bargfrede[1,2], Manopriya Chokkalingam[2], Maike Neutzer[1,2], Michael Ignarski[1,2], Thomas Benzing[1,2,4], Andreas Beyer[2,5], Bernhard Schermer[1,2], Collin Y. Ewald[3], Francesca Fabretti[1,2], Roman-Ulrich Müller[1,2,4#]

1 Department II of Internal Medicine and Center for Molecular Medicine Cologne, University of Cologne, Faculty of Medicine and University Hospital of Cologne, Cologne, Germany.

2 Cologne Excellence Cluster on Cellular Stress Responses in Aging-associated Diseases (CECAD), University of Cologne, Faculty of Medicine and University Hospital of Cologne, Cologne, Germany.

3 Laboratory of Extracellular Matrix Regeneration, Institute of Translational Medicine, Department of Health Sciences and Technology, ETH Zürich, Schwerzenbach, CH-8603, Switzerland

4 Center for Rare Diseases Cologne, Faculty of Medicine and University Hospital Cologne, University of Cologne, Cologne, Germany

5 Institute for Genetics, Faculty of Mathematics and Natural Sciences, University of Cologne, 50923 Cologne, Germany

*these authors contributed equally

#Correspondence:

Dr. Roman-Ulrich Müller, Department II of Internal Medicine, and Center for Molecular Medicine Cologne, University of Cologne, Kerpener Str. 62, 50937 Köln, Germany. Phone: +49-221-478 86288 and Email: roman-ulrich.mueller@uk-koeln.de

Abstract

The extracellular matrix (ECM) is a pivotal three-dimensional network crucial for tissue organization, cellular communication, and fundamental cellular processes, where collagens are the major chemical entity in amount. ECM deregulation is directly involved with several pathologies, such as tumour growth and invasiveness, atherosclerosis, and diabetic nephropathy. Mutations in the von Hippel-Lindau tumour suppressor (pVHL) cause VHL syndrome, a multi-tumour syndrome commonly associated with clear cell renal carcinoma (ccRCC). Loss of pVHL is associated with the activation of hypoxia-inducible factor (HIF) signaling. Mutation of VHL-1 in the nematode *Canorhabditis elegans* has been shown to increase lifespan and stress resistance. Interestingly, considering recent findings on the involvement of collagens in the regulation of lifespan, we also observed these animals to show defects in body morphology in a HIF-1 dependent manner. Based on this finding, we established a link between HIF-1 activation upon loss of VHL-1 and ECM defects associated with alterations in collagen expression. An RNAi screen examining genes upregulated in *vhl-1* mutant worms revealed the sulfide quinone oxidoreductase *sqrd-1* to mediate the change in body morphology. SQRD-1 is essential to the HIF-1 dependent increase in several collagen genes. One of these genes, *col-88*, partly mediates both the impact of loss of VHL-1 on lifespan extension and body length. The downregulation of the uncharacterised *col-88* partially restores lifespan extension and reduces body size of *vhl-1/sqrd-1* to *vhl-1(ok161)* single mutant. This study contributes to the increasing body of evidence linking lifespan extension and the ECM and now implicates this axis in hypoxia-signaling. These findings are of special interest considering the role of ECM integrity in tumour growth and metastasis.

Author Summary

The extracellular matrix and its composing collagens are associated with a wide number of diseases, including cancer. The von Hippel-Lindau tumour suppressor (pVHL) is known to work by regulating the Hypoxia Inducible Factor (HIF) to help the organism to adapt to lack of oxygen. Mutations in pVHL are associated with tumorigenesis including clear cell renal carcinoma (ccRCC). Interestingly, previous studies have implicated the pVHL/HIF axis in the regulation of collagens and extracellular matrix (ECM) formation. The exact role of the hypoxia signaling pathway regarding ECM-associated processes has not been elucidated. However, such knowledge would be important considering the links between both HIF-signaling and ECM integrity with tumor expansion and metastasis. In this study, we found that loss of *vhl-1* in the nematode *Caenorhabditis elegans* leads to a marked ECM phenotype. This phenotype is mediated by an axis involving the sulfide quinone oxidoreductase, SQRD-1, revealing a link between hypoxia signaling, sulfur metabolism, longevity and ECM integrity. These results are both of interest to future lifespan regulation studies and may be a basis to potential ECM-related targets in tumor therapies.

Introduction

The von Hippel-Lindau tumour suppressor (pVHL) tightly regulates the Hypoxia Inducible Factor (HIF) across phylae (1,2), and HIF regulates an orchestrated expression of a plethora of genes, so that the organism can properly adapt to hypoxic conditions (1). In this regulatory network, pVHL is the substrate recognition subunit of an E3 ubiquitin ligase mediating the proteasomal degradation of the HIF alpha subunit (3,4). Much is known about how pVHL interaction with HIF-1 contributes to tumorigenesis through induction of genes known to be relevant for tumor cell growth, e.g. VEGF, TGFα, and PDGFβ (5–8). However, pVHL has also been shown to have an impact on extracellular matrix (ECM) formation and composition, both in a HIF-1 dependent and -independent manner (9–12) (13,14). This is of interest, since ECM modulation has important implications in tumor invasion and metastasis. Interestingly, ECM homeostasis seems to be linked to the aging process and anti-aging interventions as well (15). Besides, in the nematode *Caenorhabditis elegans (C. elegans)*, HIF-1 activation through loss of the nematode orthologue of pVHL (VHL-1) has been shown to induce longevity(16,17). ECM related genes have been shown to be regulated not only by pVHL/VHL-1 (18)several other well-established longevity-related transcription factors (*e.g.* FOXO3, Nrf2, TP53*)* (15). Furthermore, established longevity inducing compounds such Rapamycin, Metformin, and Aspirin do also change ECM composition in a number of model organisms (19) Most importantly, ECM modulation has been linked directly and causally to lifespan-extension in *C. elegans* (20). Interestingly, we had observed a body morphology phenotype upon VHL-1 knockout implicating a role for VHL-1/HIF-1 in *C. elegans* ECM formation. Combining targeted genetics with screening approaches we identified a novel VHL-1/HIF-1 axis which – through induction of the Mitochondrial Sulfide Quinone Oxidoreductase SQRD-1 – unifies ECM and longevity-associated phenotypes in a collagen-dependent manner.

Results

vhl-1(ok161) shows a *hif-1* dependent phenotype in body length

When working with *vhl-1(ok161)* mutants, we repeatedly observed an abnormal body morphology throughout different larval stages, when compared to wild type N2 (WT) . We confirmed this finding by applying the WormSizer plugin (21) in ImageJ, which showed significant differences in body length between *vhl-1(ok161)* mutants and WT at the larval stage 1 (L1) (**Fig 1A/B**). Considering the crucial role of VHL-1 in the degradation of hypoxia-inducible factors, we examined if this phenotype depended *on hif-1*. Regarding morphology, *hif-(ia4)* (251µm) mutants did not show an overt phenotype. Importantly, while *vhl-1(ok161)* L1 larvae (187µm) are 84µm shorter than WT worms (271µm), the double mutant *vhl-1;hif-1* (236µm) is indistinguishable from WT worms (**Fig 1B**). The length phenotype was also easily detectable in L4 larvae and was again rescued by loss of *hif-1* (**Fig 1C**). The phenotype was limited to differences in length; width of both L1 and L4 larvae showed no significant differences (Suppl. **Fig. 1A** and **1B**). We went on to test whether the phenotype would have an impact on the formation of dauer larvae, a highly resilient larval stage of the nematode which develops upon stress. *vhl-1(ok161)* dauers indeed were resistant to 1% SDS after starvation (Suppl. **Fig. 1C**), even though a smaller number of *vhl-1(ok161)* animals would go into the dauer stage when compared to WT. However, again in a *hif-1* dependent manner, these animals differed morphologically from a regular dauer animal and were shorter than WT dauers (**Fig. 1D** and **E**). Taken together, loss of *vhl-1* induces a *hif-1* mediated body morphology phenotype across different developmental stages of the nematode.

131 **Figure 1. *vhl-1(ok161)* mutation shortens *C. elegans* body in a *hif-1* dependent manner**

132 **A)** Representative images of L1 WT worms, *vhl-(ok161)*, *hif-(ia4)* and *hif-(ia4)*;*vhl-(ok161)*. The scale bar represents
133 20µm; **B)** Length of L1 worms; **C)** Length of L4 worms; **D)** Representative images of dauer stage WT *vhl-(ok161)*, *hif-*
134 *1(ia4)* and *hif-1(ia4)*;*vhl-1(ok161)*; **E)** Length of dauer worms; Each point reflects the length of a single worm. The three
135 dots represent the mean of three independent experiments, while the black line represents the mean of these three
136 experiments. Significance was calculated by comparing the mean value of the three independent experiments by a
137 One-Way ANOVA followed by a Tukey post-hoc. ns = not significant, *** = $p<0.001$, * = $p<0.05$.

138

139 **Transcriptome analyses link HIF-signaling to changes in collagens and other genes**
140 **involved in the regulation of extracellular matrix formation**

141 To identify potential mediators contributing to the shorter size observed in *vhl-1(ok161)*
142 mutants, we acquired RNAseq data from these mutants compared to N2, as well as, from *hif-*
143 *1(ia4)* and the *vhl-1;hif-1* double mutants. **Fig 2A** displays the Z score transformed gene
144 expression per sample for all regulated genes (as by ANOVA and a $p<0.05$). Hierarchical
145 clustering separated *vhl-1* from both WT and *vhl-1;hif-1* worms. The analysis resulted in three
146 clusters of genes, two of which (red and blue) appeared to be clearly *hif-1* dependent.

147 Interestingly, in a Gene Ontology analysis for Molecular Function in Cluster 1 containing
148 genes which were upregulated upon loss of *vhl-1* in a *hif-1* dependent manner (**Fig 2B**),
149 "structural constituent of cuticle" was among the top 8 enriched GO-terms. We examined the
150 expression pattern of collagen-encoding genes in *vhl-1(ok161)* mutants. We observed that *vhl-*
151 *1(ok161)* mutants have an overall upregulation of all collagen genes on average, which is
152 reversed by addition of *hif-1(ia4)* mutation (**Fig. 2C)**. Collagen genes are mostly represented in
153 Cluster 1 (**Fig. 2E**), where they sum over 2/3 of all collagen genes detected when compared to
154 the whole dataset. Also, all genes that fall under the umbrella of extracellular matrix
155 components (including collagens, but also proteoglycans and glycoproteins (22)), the
156 matrisome, were regulated in a similar manner (**Fig. 2D**) and genes associated with a dumpy

157 phenotype (22) showed a similar pattern (**Suppl. Fig. 1A**). By contrast, this was not the case for
158 genes associated with other ECM phenotypes such as ''Long (lon)'' and ''Roller (rol)'', which are
159 defined by an elongated body and a helically twisted body, respectively (**Suppl. Fig. 1B** and **C**).
160 In conclusion, loss of *vhl-1* induces *hif-1* dependent changes in ECM-associated transcript
161 abundance.

162

163 **Figure 2. RNAseq data reveals a global change in the expression of collagen genes**

164 **A)** RNAseq heatmap. The Z score transformed gene expression per sample for all differentially regulated genes
165 (ANOVA, adj. p-value < 0.05) is displayed. Columns are samples, rows are genes. The first cluster, depicted in red,
166 depicts genes that are highly expressed in *vhl-1(ok161)* mutant; **B)** Gene Ontology Molecular Function (GOMF) of
167 RNAseq data. Top eight GO-terms with the highest enrichment factor. Numbers indicate proteins in the category
168 followed by category size; **C)** Log2 fold change of all *C. elegans* collagen genes detected in our RNAseq data for each
169 genotype; **D)** Log2 fold change of extracellular matrix components (matrisome (22,23)) genes detected in our RNAseq
170 data for each genotype; **E)** Collagen genes distribution of clusters 1-3. Significance was calculated by comparing the
171 mean value of the three independent experiments by a One-Way ANOVA followed by a Tukey post-hoc. ns = not
172 significant, **** = p<0.0001

173

174 **Extracellular matrix composition and functionality is altered in *vhl-1(ok161)* mutants**

175 To confirm whether the increased collagen gene expression changes in the profile of
176 expression of overall collagen genes would impact total collagen on the protein level in *C. elegans*
177 *vhl-1(ok161)* mutants, we measured total collagen by colorimetric quantification of hydroxyproline,
178 a relatively specific marker due to the abundant common proline hydroxylation events in collagens
179 (24) Adult *vhl-1(ok161)* mutants showed higher levels of hydroxyproline than WT (**Fig. 3A**)
180 Consistent with that worms with a mutation in the insulin/IGF-1 receptor *daf-2*, for which an
181 increase in collagen levels had previously been shown (20), were used as a positive control (**Fig.**
182 **3A**). Furthermore, a highly expressed and well-established collagen reporter, *col-19*p::*col-*
183 *19*::GFP, is more abundant at protein levels in day 8 adult (D8) *vhl-1(ok161)* mutants (**Fig. 3B**

184 and **3C**), while D1 adults did not show a change in the levels of this fusion protein presumably
185 since the *col-19* expression starts at the transition from the last larval stage L4 to D1 adults
186 (**Suppl. Fig 2A** and **B**).

187 We continued to assess the impact of these gene expression changes on cuticle
188 functionality, the primary component of nematodes made up by collagen and determining body
189 shape (25). This was examined using Hoechst staining, a dye which is membrane permeable but
190 does usually not permeate the cuticle (26). In contrast to WT, *vhl-1(ok161)* animals displayed
191 abnormal Hoechst positivity in the head (**Fig. 3D** and **E**), suggesting that the cuticle is defective
192 [25,26]. Again, loss of *hif-1* fully rescued the phenotype of *vhl-1* mutant worms and *hif-1(ia4)* single
193 mutants did not show differences to WT. It is interesting to notice that our *vhl-1(ok161)* mutants
194 are long-lived and heat stress resistant (17), but we have recently accessed their stress resistance
195 against paraquat and observed that indeed they are less resistance to that toxicant (**Suppl. Fig.**
196 **2C**). To address the question whether loss of *vhl-1* would lead to overt structural alterations of the
197 cuticle, we investigated different reporters of cuticle structure. However, we did not observe any
198 apparent changes for MUP-4::GFP (transmembrane protein required for epithelial cell and
199 cuticular matrix attachment), AJM-1::GFP (superficial shape of seam epidermis), and SCM::GFP
200 (seam cells, responsible to synthesizing the alae, distinctive region above the seam cells) (**Suppl.**
201 **Fig. 2D-F**). Taken together, these data suggest that *vhl-1(ok161)* related expression changes in
202 collagen genes may - while lacking gross changes in cuticle morphology - result in functional
203 cuticle permeability defects.

204

205 **Figure 3: *vhl-1(ok161)* mutants ECM is functionally impaired**

206 **A)** Hydroxyproline colorimetric measurement in day one old WT, *vhl-1(ok161)*, and *daf-2* (e1370); **B** and **C)**
207 Representative Western blot images and densitometry measurements of anti-GFP stainings of *col-19*p*::col-19::*GFP
208 reporter in WT and *vhl-1(ok161)* backgrounds in day 8 old adult worms; **D** and **E)** Fluorescence measurement and
209 representative images of Hoechst diffusion into the cuticle of different genotypes in D1 worms; Significance was

210 calculated by comparing the mean value of the three independent experiments by an One-Way ANOVA followed by a
211 Tukey post-hoc. * = p<0.05, ** = p<0.01, *** = p<0.001.
212

213 **Hypodermal expression of VHL-1 partially rescues body length**

214 We went on to confirm that the phenotype observed was indeed mediated by loss of *vhl-*
215 *1* and to address the question whether expression of *vhl-1* was required in specific cell types
216 regarding the ECM phenotype. Using a transgene driven by the *vhl-1* promoter fully rescued body
217 length in *vhl-1* mutants and overexpression of VHL-1::GFP did not affect morphology in wildtype
218 worms (**Fig. 4A** and **4B**). VHL-1::GFP was expressed all over the body with a subcellular
219 localization that was not restricted to the cytoplasm but also present in the nucleus (**Suppl. Fig**
220 **4A**). Ubiquitous overexpression of VHL-1::GFP in *vhl-1(ok161)* worms also lead to the recovery
221 of the expression of genes highly regulated upon loss of *vhl-1* (**Fig. 4C**). None of the tissue-
222 specific promoters (*elt-2p* – intestine; *unc-119p* – neurons; *dpy-7p* hypodermis) driving *vhl-1*::GFP
223 expression could recover the size of the animals (**Suppl. Fig 3B-D**); although a trend was seen
224 for hypodermis-specific expression. However, a full rescue indeed depended on more widespread
225 expression as driven by the endogenous promoter of *vhl-1*. Therefore, we can conclude that *vhl-*
226 *1(ok161)* mutants' abnormal size is due to *vhl-1* loss of function, and that no singular tissue-
227 specific rescue is able to restore body size, which is only achieved with full body expression.
228

229 ***sqrd-1* contributes to the effect of HIF-activation on body length**

230 Next, we aimed to pin down downstream effectors underlying the impact of *vhl-1* mutation
231 on morphology. Based on the RNAseq data, we selected 20 genes strongly positively regulated
232 in *vhl-1* mutants in a *hif-1* dependent manner. Based on RNAi clone availability, these genes were
233 included in an RNAi screen for body size (**Suppl. Table 1**). To check if the phenotype was
234 reversible at all by RNAi, we first performed an experiment using *hif-1* RNAi. Notably, this
235 approach (in contrast to the mutant) only partially rescued the length of the animals (**Suppl. Fig.**

236 **3E**). Therefore, partial rescue of size was considered as the benchmark for our screen, and we
237 proceeded with 15 candidate genes. The knockdown of one of these genes, partially, but
238 consistently (n=3), recovered length, the Sulfide Quinone Oxireductase (SQOR) *sqrd-1* (**Suppl.**
239 **Fig. 3E**).

240 The recovery of the short phenotype of *vhl-1(ok161)* worms was considerably
241 higher when we crossed them with a loss of function mutant of *sqrd-1* (mr28) (*vhl-1* 155µm
242 x 186µm *vhl-1/sqrd-1*) (**Fig. 4D** and **E**). *sqrd-1* (mr28) worms do not differ from WT
243 regarding body length. *sqrd-1* was indeed also one of the most strongly regulated genes
244 in our RNAseq dataset (*vhl-1* vs WT log2 Fold Change: 3,64909, p=0,00005). Its
245 expression levels, together with 2 ECM-associated genes chosen from the RNAseq
246 dataset were fully restored by the overexpression of *vhl-1* in the *vhl-1*p::*vhl-1*::GFP
247 transgenic animal (**Fig. 4C**). Taken together our data suggest that *sqrd-1* is a *hif-1* target
248 that is at least partially responsible for the body morphology phenotype of *vhl-1(ok161)*
249 mutant worms. Collagen had previously been linked to longevity in the nematode model
250 (20) and *vhl-1* mutant worms are known to be long-lived (17). Interestingly, when
251 measuring lifespan, we observed that the long lifespan of *vhl-1(ok161)* animals was
252 completely reversed back to WT in the *vhl-1/sqrd-1* double mutant (**Fig. 4F**). Taken
253 together these data suggest that *sqrd-1* is be an important downstream effector of *vhl-1*
254 KO not only regarding body size, but also lifespan.

255

256 **Figure 4: *sqrd-1* is partially responsible for *vhl-1(ok161)* phenotypes**

257 **A)** Representative images of L1 *vhl-1(ok161)* rescue by *vhl-1*p::*vhl-1* construct; **B)** Size quantification of *vhl-1(ok161)*
258 L1 mutants and *vhl-1p*::*vhl-1*::GFP rescue; **C)** mRNA expression levels of three strongly upregulated genes in *vhl-*
259 *1(ok161)* in comparison to *hif-1(ia4)* and *vhl-1p*::*vhl-1*::GFP rescue; **D)** Size quantification of F1 generation L1 worms
260 after *hif-1* RNAi exposure in P0; **E)** Size quantification of different L1 mutant animals, including *sqrd-1* (mr28) and

261 double mutants *vhl-1(ok161)*/*sqrd-1* (mr28); F) Lifespan of different mutants. N = WT: 198, *vhl-1*: 278, *sqrd-1:* 203, *vhl-*
262 *1/sqrd-1*: 317 Significance was calculated by comparing the mean value of the three independent experiments by a
263 One-Way ANOVA followed by a Tukey post-hoc or a survival Kaplan-Meier analysis. * = p<0.05, ** = p<0.01, *** =
264 p<0.001, **** = p<0.0001, ns = non-significant
265

266 ***The effect of sqrd-1 regarding body length and longevity of vhl-1 mutant worms depends***
267 ***on col-88***

268 Considering that *sqrd-1* may mediate its effects on body morphology through collagens, we
269 selected the top 5 most upregulated collagen genes in our RNAseq data of *vhl-1(ok161)* worms
270 (**Suppl. Table 2**), and analyzed them for body size and *sqrd-1* epistasis by the means of mRNA
271 expression. While knockdown of three of the collagen genes were able to slightly, but significantly
272 increase *vhl-1* worm size (**Fig. 5A**), only one of these was differentially regulated in a manner that
273 suggested epistasis with *sqrd-1* and *vhl-1,* being upregulated in the *vhl-1(ok161),* and
274 downregulated in *sqrd-1* (mr28) and *vhl-1/sqrd-1* double mutant (**Fig. 5B**): *col-88* (**Fig. 5A** and **B,**
275 **Suppl. Fig. 4A**). Indeed, RNAi-mediated knockdown of *col-88*, resulted in an indistinguishable
276 body length between *vhl-1* mutants and *vhl-1;sqrd-1* double mutant worms (**Fig. 5C**) and mean
277 lifespan (**Fig. 5D**). In conclusion, *col-88* seems to be positively regulated by *sqrd-1*, which in turn
278 is upregulated upon *vhl-1* deletion/HIF-1 activation, seemingly leading to reduced body size in
279 *vhl-1*(ok161) mutants.
280

281 **Figure 5: *col-88* acts downstream of *sqrd-1* regarding body length and longevity of *vhl-1* mutant worms**
282 **A)** Body length upon exposure of P0 to 5 RNAi collagen clones that were upregulated in *vhl-1(ok161)*, followed by
283 wormsizer analysis on F1 L1 newly hatched worms**; B)** mRNA expression levels of *col-88* in L1 and L4 animals in
284 different genetic backgrounds; **C)** Body length of F1 generation L1 mutant worms after *col-88* RNAi exposure in P0; **D)**
285 Lifespan of different mutants in RNAi bacteria for *col-88* or empty vector (L4440). N= WT 245, *sqrd-1* 308*, vhl-1* 289,
286 *vhl-1/sqrd-1* 277, *vhl-1* (EV) 146. Significance was calculated by comparing the mean value of the three independent
287 experiments by a One-Way ANOVA followed by a Tukey post-hoc. * = p<0.05, ** = p<0.01, *** = p<0.001, ns = non-
288 significant

289 **Discussion**

290 Here we present evidence for the link in between the hypoxia pathway regulator von
291 Hippel-Lindau, VHL/*vhl-1,* and collagens to ultimately control body size and lifespan. Our data
292 points to the participation of a sulfide metabolism related protein, the sulfide quinone
293 oxidoreductase 1 SQOR/*sqrd-1,* as an important mediator to control these phenotypes. While
294 sqrd-1 expression is induced by HIF-1, a specific collagen (*col-88*) appears to act downstream of
295 *sqrd-1*.

296 pVHL has previously been implicated as a player in the regulation of ECM biology and
297 integrity (11). However, a direct functional link has not been fully elucidated. Previous results
298 pointed towards ECM association being a mainly HIF-independent phenotype. In fact, VHL has
299 been shown to act independently of HIF-1 when it comes to its interaction with collagen 4 alpha
300 2 (COL4A2) and its proper assembly into the extracellular matrix (27). In contrast, our data clearly
301 show HIF-dependence for both body length and ECM integrity. However, our results do not rule
302 out HIF-independent ECM-associated roles of pVHL. Interestingly, *vhl-1;hif-1* double mutants
303 appeared to be slightly shorter than WT or hif-1 mutant worms. Yet, this difference did not reach
304 statistical significance anymore, so future studies will need to examine this question in more detail
305 The abnormal Hoechst uptake – as well as the paraquat sensitivity – point towards defects in
306 cuticle integrity, a finding that has been previously observed upon deletion of collagens *dpy-9* and
307 *dpy-10* (28). However, our results cannot rule out that intestinal leakiness contributes to this result.
308 Again, such a phenotype may involve changes in collagen composition of the basement
309 membrane, but may also be a consequence of defective intestinal cell-cell junctions (29,30)).

310 The small body size persists through several rounds of molting and is independent of
311 starvation, since larval stage 4 animals (not starved) display a short phenotype which is recovered
312 upon *hif-1* (ia) deletion (**Fig. 1C**). Not only regular larval stages, but the radically different
313 quiescent dauer larvae size is also changed by *vhl-1(ok161)* mutation. This finding indicated that
314 the causal factor for body changes had to be a widely common biomolecule, such as structural

315 parts of the cuticle, such as collagens. In that direction, *cut-6* knockdown, predicted to encode a
316 structural part of the cuticle, induces similar changes in dauer larvae, resulting in a dumpy
317 phenotype (31). In this regard, collagens are not only a major component of *C. elegans* cuticle
318 (25), but are associated with well-studied worm phenotypes associated with short body length,
319 such as Sma (small) and Dpy (dumpy) (25,32), and Dpy associated genes were in fact regulated
320 in *vhl-1(ok161)* mutants in a *hif-1(ia4)* dependent manner (**Suppl. Fig. 1A**). The induction of
321 collagens upon loss of *vhl-1* could be recapitulated on the protein level, both when quantifying
322 overall collagen levels or *col-19* as an example for one specific collagen. Importance of these
323 changes for ECM biology is not only shown by the change in body length but also reflected by
324 defects in cuticle integrity in *vhl-1* mutant worms.

325 Using an RNAi screen for downstream mediators of the body length reduction among HIF-
326 induced genes (**Suppl. Table 1** and **Suppl. Fig. 3E**), we identified a rather unexpected gene, the
327 sulfide quinone oxireductase 1, *sqrd-1*. *sqrd-1* is the orthologue of mammalian SQOR, and
328 encodes a mitochondrial sulfide quinone oxidoreductase responsible for the first step of the
329 conversion of sulfides into less toxic persulfides (33,34). In *C. elegans* it has been described to
330 be required for survival under toxic concentrations of hydrogen sulfide (H_2S) (34), meaning its
331 deletion hinders *C. elegans* sensitive to this gas, similarly to HIF-1 deletion (35,36). Interestingly,
332 one previous study found that HIF-1 activation after H_2S exposure was exclusive to the
333 hypodermis and independent of *vhl-1* (35).

334 Even though link has not been fully understood, the relationship between H_2S and ECM
335 remodeling has been documented. As an example, spontaneously hypertensive rats treated with
336 H_2S donor Na_2HS did not produce as much collagen 1, collagen 4, and hydroxyproline in their
337 vascular smooth muscle cells (37). Similarly, H_2S deficiency is key to ECM remodeling in diabetic
338 kidney, whereas treatment with the H_2S donor GYY4137 is able to repress collagen 1 and 4
339 overexpression in a mouse model (38). Additionally, pulmonary and liver fibrosis progression
340 seem to also have endogenous H_2S levels decreased, whereas the treatment with donors can

341 have mild ameliorative effects (39,40). Interestingly, hypoxia itself, as well as pVHL inactivation
342 in ccRCC, are known to correlate with buildup of intracellular H_2S (41–44)H_2S is considered a
343 modulator of HIF-1 (45–47), and may contribute to tumor survival and progression (41). Whether
344 this gasotransmitter is a consequence or just a collateral in these scenarios is yet to be clarified,
345 since the regulation of the pathway that controls the production of this gas, and even small
346 molecules that are able to produce it at variable rates, amounts, and with cellular compartment
347 specificity, could be further explored as potential therapeutic targets for diseases that involve HIF-
348 1 activation, hypoxia, or pVHL inactivation (38,48). In that sense, we believe that our work sheds
349 further light onto this topic, demonstrating the necessity of a sulfide catabolism related gene in an
350 ECM-related phenotype regulated by HIF-1.

351 *C. elegans* possesses 181 collagen-coding genes(49) ,and the redundancy in between
352 them is not as big as one would expect. A recent study screened 93 collagen genes by means of
353 RNAi and only 6 of these genes were associated to a cuticle barrier defect (28). Knockdown of
354 two of these genes, *dpy-9* and *dpy-10,* did not only made the cuticle permeable, but also increased
355 the uptake and toxicity of the stressor paraquat over adult animals. Consequently, increased
356 stress resistance may also be one of the links between collagens and lifespan extension.

357 *Vhl-1(ok161)* mutant worms are known to be both stress resistant and long-lived (17), and
358 longevity in this strain is mediated by HIF-1. Interestingly, an unexpected link between collagens
359 and longevity had previously been established in long-lived *daf-2* (e1370) mutants (20). This
360 mechanism is not specific to longevity mediated by inhibition of insulin signaling but was also
361 shown for caloric restriction induced by *eat-2* mutation, or germline ablation via *glp-1* knockout
362 (20). Interestingly, one of the collagens examined in our study, *col-19*, was not induced before
363 later adulthood. In line with the direct connection between collagen expression and lifespan, we
364 could now show that *sqrd-1* dependent induction of a specific collagen – col-88 – was required
365 for the lifespan extension in *vhl-1* mutant worms.

366 Based on its amino acid sequence COL-88 is predicted to be structural part of the cuticle,
367 and it was first identified in a RNAi screen for osmotic hypersensitivity (50). To the extent of our
368 knowledge, no other study has described any specific COL-88 function or associated phenotype.
369 We believe that the upregulation of this specific collagen plays an important role in *vhl-1* body
370 size, probably playing a role in ECM overall organization. SQRD-1 is central to the metabolism of
371 H_2S. Since H_2S is an important mediator of lifespan in different species under caloric restriction
372 (51), and H_2S donors are known for improving stress resistance and lifespan in *C. elegans* (52–
373 54), one could speculate that the effects of this gasotransmitter on lifespan and stress resistance
374 is also ECM remodeling, consequently affecting body size. Recently, it has been shown that H_2S
375 donors targeted specifically to the mitochondria can induce collagens (Type I) on the protein and
376 mRNA level in normal human dermal fibroblasts (NHDFs) and mouse skin in vivo to protect
377 against UV induced damage in an Nrf2 dependent manner (55).
378 Novel elasticity measurements have recently revealed that older worms become ''stiffer''
379 while long lived *daf-2* animals were still more elastic in their cuticle structure at the same age,
380 while the knockdown of *col-120* was able to ablate *daf-2* elasticity and lifespan (20,56). Similarly,
381 collagens seem to be the most significantly altered group of proteins in the proteome of the long-
382 lived germline loss model *glp-1* (e2141) (57), where, interestingly, H_2S levels are increased, and
383 its main source of production, the transsulfuration pathway, is required for lifespan extension (58).
384 Taken together, our data and the studies mentioned point to a possible new link in between H_2S
385 metabolism, ECM composition and longevity. It will be intriguing to further characterize this link in
386 future studies and to extend the work to mammalian models. Such knowledge will be of special
387 interest regarding the role of the pVHL/HIF-axis in tumorigenesis considering the importance of
388 the ECM to tumor growth and metastasis.
389
390
391

392 **Materials and Methods**

393

394 ***C. elegans* strains and maintenance**

395 The following strains have been used in this study: *C. elegans* Bristol N2 (WT);
396 CB5602 [*vhl-1(ok161)* X]; ZG31 [hif-1(ia4)]; AR13 [*sqrd-1* (mr28) IV]; TMB031 [*hif-1*(ia4)
397 V; *vhl-1*(ok161) X]; CB1370 [daf-2 (e1370) III]; TP12 [kaIs12 (*col-19*::*gfp*)]; JR667 [*unc-119*
398 *(e2498::Tc1) III; wIs51* (*SCMp::*gfp*;unc-119+)*] V]; TBM033 [*vhl-1(ok161)* X; kaIs12 (*col-*
399 *19*::*gfp*]; TMB036 [*jcIs* (*ajm-1*::*gfp*;*unc-29*+;*rol-6* (su1006) IV; *vhl-1(ok161)* X]; AA813
400 [*jcIs1* (*ajm-1*::*gfp*;*unc-29*+;*rol-6* (*su1006*) IV]; TMB101 [*vhl-1(ok161)* X; *sqrd-1* (mr28) IV].
401 All strains were provided by the *Caenorhabditis* Genetics Center (University of Minnesota,
402 Twin Cities, MN, USA). CGC strains have been outcrossed into our WT background at
403 least 2x. All strains named under "TMB" have been generated in our lab. Genotypes were
404 confirmed by using the primers included in **Suppl. Table 3**.

405 Worms were handled and maintained at 20 °C on NGM (nematode growth
406 medium)/*Escherichia coli* OP50 Petri dishes. NMG was prepared with 3g/L of NaCl,
407 2,5g/L of Bacto Peptone, and 18g/L of Bacto Agar. After autoclaving 25mM of KPO_4,
408 0.005mg/mL Cholesterol, 1mM $MgSO_4$, and 1mM of $CaCl_2$ were added. *E. coli* OP50
409 bacteria were grown overnight (12-16h) from a single colony. O.D. was adjusted to 1.5
410 with LB media (20g/L) by measuring density at 650nm.

411 Age synchronized populations used for experiments were obtained by isolating
412 embryos from gravid hermaphrodites using bleaching solution (1% NaOCl; 0.25 M
413 NaOH), followed by neutralization with M9 buffer (KH_2PO_4 12g/L, Na_2HPO_4 24g/L, NaCl
414 20g/L, $MgSO_4$ 1mM). The axenization of the worms has been done by employing the
415 same bleaching solution over a small group of pregnant hermaphrodites if contamination

416 was spotted. All experiments were conducted at 20±0.5ºC in a humidified-controlled
417 environment. No ethical approval was needed.
418
419 **RNAi**
420 *E. coli* HT115 (DE3) transformed with the L4440 vector, empty or including dsRNA
421 specific to the gene which knockdown is intended, were inoculated in LB medium
422 containing 100µg/mL of ampicillin and 12,5µg/mL of tetracycline overnight. The next day,
423 the medium was concentrated to a 600nm O.D. of 1,5, upon which 1mM of the expression
424 inducer IPTG (isopropyl β-D-1-thiogalactopiranoside) was added, besides being already
425 present at the same concentration inside the NGM medium in which bacteria were seeded
426 as a food source for *C. elegans*.
427
428 **Body size measurement**
429 Age synchronized L1 populations were obtained by bleaching a large plate with
430 pregnant hermaphrodites (D0) either on regular OP50 *E. coli* (experiments comparing
431 different knockouts) or fed with HT115 (DE3) *E. coli* carrying different RNAi clones (for
432 experiments carried after knockdown). These populations have either been allowed to
433 grow until they reached the L4 (48h after bleaching) stage or placed in unseeded plates
434 so that L1 animals were measured (16h after bleaching). The WormSizer plugin was used
435 to analyze the length and width of the worms. Worms were imaged at 63x magnification
436 using an Axiozoom (Zeiss) microscope. At least 50 worms per group were imaged per
437 biological replicate. Measurements were manually reviewed after WormSizer analysis to
438 exclude potential confounders (e.g. any debris, bacterial lawn, or incorrectly selected
439 worm).

440 **Dauer formation assay**

441

442 Age synchronized 500 L1 animals were placed either in NGM plates containing
443 OP50 or no food source. OP50-containing plates were kept at 20°C and plates with no
444 food source were kept at 25°C to induce dauer formation. After 3 days we have washed
445 the animals with M9 buffer and treated them with 1% SDS for 30min. After the treatment
446 the animals were washed 3x with M9 buffer and placed in a OP50-containing NGM plate
447 and let to rest for 24h. The animals were scored and the percentage of survival was
448 estimated based on the initial number of animals placed in each plate (500).

449

450 **Preparation of RNA samples, RNA extraction and sequencing**

451 Synchronized worms were grown according to their optimum growth requirements
452 and collected at their D1 adult stage in Trizol (Invitrogen) in three independent biological
453 repeats. Total RNA was extracted using RNeasy Mini spin column (QIAGEN).
454 Concentration and purity of the RNA was measured by NanoDrop. polyA+ mRNA was
455 isolated from total RNA with NEBNext Poly(A) mRNA Magnetics Isolation Module (New
456 England Biolabs). RNA-Seq libraries were prepared with NEBNext Ultra Directional RNA
457 Library Prep Kit for Illumina (New England Biolabs). Capillary electrophoresis (Agilent
458 Bioanalyser and Agilent Tapestation) was used to assess quality and quantity at all steps.
459 Libraries were quantified by fluorimeter, immobilized and processed onto a flow cell with
460 a cBot (Illumina) followed by sequencing-by-synthesis with TruSeq v3 chemistry on a
461 HiSeq2500 performed at the Max Planck Genome Center CGC (Cologne, Germany).

462

463 **Bulk RNA sequencing analysis**

464 The reads were trimmed with Trimmomatic (version 0.36) (59) using default
465 parameters. The trimmed reads were mapped to the WBcel235 Caenorhabditis elegans
466 reference genome with STAR version 2.6.0 (60) using default parameters. The analysis
467 of differential gene expression was performed using the R package DeSeq2 (version
468 1.26.0) (61,62). For visualization purposes the batch effect was removed using the
469 method removeBatchEffect from the R package limma (63). The enrichment analysis was
470 done using the R package topGO (64,65). For the heatmap and clustering the R package
471 pheatmap was used (66).

472 Bulk RNA sequencing data are available in the ArrayExpress database
473 (https://www.ebi.ac.uk/biostudies/arrayexpress) under accession number E-MTAB-
474 13659 (reviewer only link: see separate data availability statement).

475 **Collagen analysis**

476 Synchronized L1 larvae were placed on 9 cm NGM plates containing OP50
477 bacteria at 20°C and kept there till they reached the L4 stage (48h). Larvae were washed
478 from the plates and transferred to new 5-Fluoro-2'deoxyuridine (FUdR) containing plates
479 till day 1 or day 8 of adulthood. At those time points, the remaining animals were
480 harvested by washing 3x with M9 buffer. 3000 worms per strain and condition were used
481 for the assay. Collagen levels were determined using the *QuickZyme* Biosciences Total
482 Collagen Kit (QZBTOTCOL1), which detects Hydroxyproline, according to the
483 manufacturer's instructions. Briefly, hydroxyproline is quantified at 570nm after being
484 conjugated with chromophore. Values are displayed as µg/mL.

485

486 **Western blotting**

487 Western blot analysis was used to measure the expression of the GFP reporter.
488 First, 50 worms were picked into 1 ml lysis buffer and sonicated ten times for 30 seconds.
489 Afterwards 2xLaemmli buffer (150 mM TrisHCl pH 6,8, 4% SDS, 20% Glycerol, 0.002%
490 Bromophenol blue, 0.1 M DTT) was added and the sample was incubated for 5 minutes
491 at 95°C. 30 µl of the samples were loaded on a 4 to 12% Bis-Tris polyacrylamid gel and
492 the gel was run at 200 V constant for 60 minutes. Gels were transferred to PVDF
493 membranes. Staining was performed using an anti GFP antibody (Santa Cruz, sc-8334,
494 1:5,000) and an anti-rabbit secondary antibody (1:15,000, Jackson ImmunoResearch,
495 711-165-152). Visualization was performed using Femto Luminol (Invitrogen) and a
496 chemiluminescence imaging system (FusionSolo, PeqLab).

497

498 **Epifluorescence visualization and image acquisition**

499 A Zeiss Axiovert 200 microscope (Zeiss, Jena, Germany) equipped with a Plan
500 Apochromat 20x objective and a GFP filter set was used for fluorescence microscopy. All
501 pictures were taken using this microscope, except for worms treated with the Hoechst
502 staining for which the confocal microscope (Zeiss Meta 710, Type Confocal Laser
503 Scanning Microscope 20x objective) was used. The AXIO Zoom.V16 was used to take
504 the pictures for the WormSizer plug-in and to pick GFP fluorescent worms. The AXIO
505 Zoom.V16 was equipped with an objective from ZEISS (PlanNeoFluar Z 1x/0.25 FWD 56
506 mm), with a filter set at 74 HE, and with a Leica DFC450 camera. Worms were mounted
507 onto 2% agar pads and paralyzed with 15mM levamisole. Fluorescence measurement
508 was calculated as CTCF (Corrected Total Cell Fluorescence).

509

510 **Cuticle permeability assay**

511 To analyze the permeability of the worms' extracellular matrix, Hoechst staining
512 was performed as previously described (67). Briefly, young adults were placed in 1.5 ml
513 tubes with 1 ml M9 buffer containing 1µg/ml Hoechst 33342 and incubated for 15 minutes
514 at RT. After washing three times in M9, worms were immobilized using 60 mM Sodium
515 Azide on 2% agarose pads and imaged at the confocal microscope keeping acquisition
516 parameters constant for intensity comparison. The tail region was analyzed to access
517 oral/intestinal absorption, while the head region was analyzed to access cuticle
518 absorption.

519

520 **Generation of transgenic lines by DNA bombardment**

521 Transgenic lines for reexpression of *vhl-1* under its endogenous promoter were
522 generated by bombarding *unc-119 (ed3)* worms with plasmid harboring the *vhl-1*::GFP
523 transgene under the control of *vhl-1* promoter and *unc-119* as a selection marker. 30mg
524 of gold particles (Gold powder 0.3-3micron/99.9% from chemPUR) were transferred in a
525 1.5mL tubes (DNA LoBind, Eppendorf), vortexed with 1mL 70% EtOH for 5min, incubated
526 for 15min at room temperature, and shortly spun down so that the supernatant could be
527 discarded. Gold particles were washed three times with 1mL of water and resuspended
528 in 500µL of 50% glycerol for a 60mg/mL concentration of the particles. This stock solution
529 was coated with plasmid DNA containing the construct of interest by vortexing it for 5min
530 and mixing 20µL of its supernatant with 10µL of 1-2mg/mL solution of plasmid DNA and
531 vortexing the mix for 1min. 300µL of 2.5M $CaCl_2$ was added over the mix, vortexed for

532 1min, followed by 300µL of 2.5M $CaCl_2$ and 3 more minutes of vortexing. The particles
533 were centrifuged at 12000rpm for 1min and washed with 800µL of 70% EtOH, centrifuged
534 again and washed with 500µL of 100% EtOH, and finally washed one last time after
535 centrifugation with 80µL of 100% EtOH. This solution was distributed on 7 macrocarriers
536 and allowed to dry.

537 Briefly, a mixed population of adults (D0-D2 adults) were cultured in EP (peptone
538 enriched) plates, collected using M9 and further transferred to cold unseeded 10cm NGM
539 plates. Plates with animals were placed in the gene gun (Model PDS-1000/He Biolistic
540 Particle Delivery from BIO-RAD) with gold particles that were previously coated with *vhl-*
541 *1p::vhl-1::*GFP plasmid DNA. After bombardment the worms were washed off the plates
542 and distributed on 10cm NGM plates seeded with OP50 *E. coli* and incubated at 20°C:
543 After two weeks only the worms containing the *unc-119* rescue, and consequently our
544 construct of interest, were able to enter the dauer stage due to starvation. We confirmed
545 transgene presence by detecting GFP by microscopy and PCR.

546

547 **Plasmid construction and microinjection**

548 Tissue specific rescue was achieved by cloning chosen promoters into pdest-
549 MB14 plasmid, which includes GFP in frame. Briefly, *vhl-1* entire genomic sequence was
550 cloned plus a 50bp region upstream of the *vhl-1* first codon, which should cover its
551 promoter. All primers used are included in **Suppl. Table 3**.

552 The injection was performed as described before (68) using an Axio Observer A1
553 (Zeiss [Carl Zeiss], Tornwood, NY) and FemtoJet (Eppendorf, Hamburg, Germany)
554 microinjection system. Briefly, five gravid adult worms were placed on a coverslip with a

555 dried 2% agarose pad on it and were covered with a layer of Halocarbon oil (Sigma, St
556 Louis, MO) to prevent drying during the process. The injection needle (Femtotips II,
557 Eppendorf) was filled with a mix of 5µg of the plasmid of interest and 1µg of mCherry as
558 an injection control, all diluted with Water for Injection (Ampuwa). Each worm was injected
559 in one of the two gonads, and at least 30 worms were injected with each specific plasmid.
560 After injection the worms were immediately placed on a NGM plate seeded with OP50 to
561 recover, and incubated at 20°C.

562

563 **Quantitative Real Time PCR**

564 Briefly, RNA extraction was performed with the Direct-zol RNA Miniprep kit (Zymo
565 Research) following the manufacturer's instructions. Prior to the reverse transcription by
566 using the High-Capacity cDNA Reverse Transcription kit (Applied Biosystems), RNA
567 concentration and sample quality were assessed on a Nanodrop spectrophotometer
568 (Peqlab). mRNA was assessed by SYBR Green (ThermoFisher Scientific) qPCR using
569 *act-1* as endogenous control. Primers are listed in Supplementary Table S3. The qPCR
570 experiments were performed on a QuantStudio 12 K Flex Real-time PCR System
571 (ThermoFisher Scientific). All primers used are included in **Suppl. Table 3**. For data
572 analysis, all results were normalized to the housekeeping gene *act-1* using the delta-delta
573 CT followed by a One-way ANOVA and a Tukey posthoc test ($p < 0.05$).

574

575 **Lifespan analysis**

576 All lifespan analyses were conducted using the Lifespan Machine (69) For each
577 lifespan experiment 35 young adult worms were transferred to 60 mm NGM or RNAi

578 plates containing 100µm Fluorodeoxyuridine (FUdR) to inhibit reproduction, or
579 additionally Paraquat (Methylviologen, Sigma) 10mM for stress resistance. For each
580 strain, at least 5 plates were used. The plates were put upside down without the lids on
581 the glass plate of the scanners and fit into a rubber cast (rubber mask) to prevent
582 desiccation. The animals were scanned each 30 minutes until the end of the experiment
583 (determined by the expected time at which all animals would be dead e.g. 30 days for
584 *WT*). After the end of the experiment, a storyboard containing a timeline for every animal
585 in the experiment was generated, so that their movement cessation could be manually
586 checked, as well as any other discrepancy (e.g. animal confused with artifact). The final
587 death events of the worms were collected in a table and plotted as a survival curve.
588

589 **Statistical analysis**

590 The software GraphPad Prism 9 was used for all statistical analysis conducted. *,
591 **, ***, and **** represent p values that were lower than 0.05, 0.01, 0.001, and 0.0001
592 respectively. The specific statistical tests used are specified for each experiment in the
593 figure legends and in the respective methods section.
594

595 **Acknowledgments**

596 We thank Serena Greco-Torres for excellent technical support and WormBase for curated
597 gene and phenotype information (https://wormbase.org/). Some strains were provided by
598 the *Caernohabditis elegans* Genetics Center (CGC), which is funded by NIH Office of
599 Research Infrastructure Programs (P40 OD010440). This study was supported by the

German Research Foundation (DFG MU 3629/6-1 to R.-U.M.). C.Y.E. and C.S. received funding from the Swiss National Science Foundation Funding (SNF P3 Project 190072).

Author Contributions

All authors participated in analyzing and interpreting the data and reviewed the manuscript. R.E., R.-U.M, and W.S. designed the experiments. R.E., M.N. and W.S. performed experiments. K.B., A.B. and M.C. analyzed the RNAseq data. W.S. wrote and R.E., M.I. and R.-U.M. reviewed the original manuscript. C.Y.E., S.B. and C.S. supported the setup of the lifespan machine and C.Y.E. provided scientific advice regarding the Collagen experiments R.-U.M, M.I. and F.F. supervised the work supervised the project and R.-U.M. provided funding.

Conflict of interest

The authors have no competing interests to declare. The authors declare that the research was conducted in the absence of any commercial or financial relationships that could be construed as a potential conflict of interest. With no relation to the present manuscript, C.Y.E. declares to be a co-founder and shareholder of Avea Life AG and Lichi3 GmbH and is employed by Novartis and R.-U.M. serves on the scientific advisory board of Santa Barbara Nutrients.

References

650 1. Semenza GL. Hypoxia-Inducible Factor 1 (HIF-1) Pathway. Science's STKE. 2007 Oct 9;2007(407).

651 2. Maxwell PH, Wiesener MS, Chang GW, Clifford SC, Vaux EC, Cockman ME, et al. The tumour
652 suppressor protein VHL targets hypoxia-inducible factors for oxygen-dependent proteolysis.
653 Nature [Internet]. 1999;399(6733):271–5. Available from: https://doi.org/10.1038/20459

654 3. Ohh M, Park C, Ivan M, Hoffman M, … TKN cell, 2000 undefined. Ubiquitination of hypoxia-
655 inducible factor requires direct binding to the β-domain of the von Hippel–Lindau protein.
656 nature.com [Internet]. [cited 2023 May 2]; Available from:
657 https://idp.nature.com/authorize/casa?redirect_uri=https://www.nature.com/articles/ncb0700_
658 423&casa_token=689Z3WxIJroAAAAA:ba2RFWrpRhZyuvawX9HllUy4cakzU7fODNqRQEkiA869oiQ
659 sVUCTt19RW59fyotW4piBIwIA9V7hKGALxg

660 4. Maxwell PH, Wlesener MS, Chang GW, Clifford SC, Vaux EC, Cockman ME, et al. The tumour
661 suppressor protein VHL targets hypoxia-inducible factors for oxygen-dependent proteolysis.
662 Nature 1999 399:6733 [Internet]. 1999 May 20 [cited 2023 May 2];399(6733):271–5. Available
663 from: https://www.nature.com/articles/20459

664 5. Gnarra JR, Zhou S, Merrill MJ, Wagner JR, Krumm A, Papavassiliou E, et al. Post-transcriptional
665 regulation of vascular endothelial growth factor mRNA by the product of the VHL tumor
666 suppressor gene. Proc Natl Acad Sci U S A [Internet]. 1996 Oct 1 [cited 2023 May
667 2];93(20):10589–94. Available from: https://pubmed.ncbi.nlm.nih.gov/8855222/

668 6. Kaelin WG. Molecular basis of the VHL hereditary cancer syndrome. Nature Reviews Cancer 2002
669 2:9 [Internet]. 2002 Sep [cited 2023 May 2];2(9):673–82. Available from:
670 https://www.nature.com/articles/nrc885

671 7. Reversion of deregulated expression of vascular endothelial growth factor in human renal
672 carcinoma cells by von Hippel-Lindau tumor suppressor protein - PubMed [Internet]. [cited 2023
673 May 2]. Available from: https://pubmed.ncbi.nlm.nih.gov/8625303/

674 8. Na X, Wu G, Ryan CK, Schoen SR, Di'Santagnese PA, Messing EM. Overproduction of vascular
675 endothelial growth factor related to von Hippel-Lindau tumor suppressor gene mutations and
676 hypoxia-inducible factor-1α expression in renal cell carcinomas. Journal of Urology. 2003 Aug
677 1;170(2 I):588–92.

678 9. Ohh M, Yauch RL, Lonergan KM, Whaley JM, Stemmer-Rachamimov AO, Louis DN, et al. The von
679 Hippel-Lindau tumor suppressor protein is required for proper assembly of an extracellular
680 fibronectin matrix. Mol Cell. 1998;1(7):959–68.

681 10. Singh P, Carraher C, Schwarzbauer JE. Assembly of fibronectin extracellular matrix. Annu Rev Cell
682 Dev Biol. 2010 Nov 10;26:397–419.

683 11. Stickle NH, Chung J, Klco JM, Hill RP, Kaelin WG, Ohh M. pVHL Modification by NEDD8 Is Required
684 for Fibronectin Matrix Assembly and Suppression of Tumor Development. Mol Cell Biol. 2004 Apr
685 1;24(8):3251–61.

686 12. Russell RC, Ohh M. NEDD8 acts as a 'molecular switch' defining the functional selectivity of VHL.
687 EMBO Rep. 2008 May;9(5):486–91.

688 13. Kurban G, Hudon V, Duplan E, Ohh M, Pause A. Characterization of a von Hippel Lindau Pathway
689 Involved in Extracellular Matrix Remodeling, Cell Invasion, and Angiogenesis. Cancer Res
690 [Internet]. 2006 [cited 2023 May 2];66(3):1313–22. Available from: www.aacrjournals.org

691 14. Kurban G, Duplan E, Ramlal N, Hudon V, Sado Y, Ninomiya Y, et al. Collagen matrix assembly is
692 driven by the interaction of von Hippel-Lindau tumor suppressor protein with hydroxylated
693 collagen IV alpha 2. Oncogene [Internet]. 2008 [cited 2023 May 2];27:1004–12. Available from:
694 www.nature.com/onc

695 15. Vidović T, Ewald CY. Longevity-Promoting Pathways and Transcription Factors Respond to and
696 Control Extracellular Matrix Dynamics During Aging and Disease. Frontiers in aging.
697 2022;3:935220.

698 16. Shen C, Shao Z, Powell-Coffman JA. The Caenorhabditis elegans rhy-1 gene inhibits HIF-1 hypoxia-
699 inducible factor activity in a negative feedback loop that does not include vhl-1. Genetics
700 [Internet]. 2006 [cited 2023 Apr 27];174(3):1205–14. Available from:
701 https://pubmed.ncbi.nlm.nih.gov/16980385/

702 17. Müller RU, Fabretti F, Zank S, Burst V, Benzing T, Schermer B. The von Hippel Lindau tumor
703 suppressor limits longevity. Journal of the American Society of Nephrology [Internet]. 2009 Dec 1
704 [cited 2023 Feb 23];20(12):2513–7. Available from:
705 https://journals.lww.com/jasn/Fulltext/2009/12000/The_von_Hippel_Lindau_Tumor_Suppressor
706 _Limits.9.aspx

707 18. Bishop T, Lau KW, Epstein ACR, Kim SK, Jiang M, O'Rourke D, et al. Genetic analysis of pathways
708 regulated by the von Hippel-Lindau tumor suppressor in Caenorhabditis elegans. PLoS Biol
709 [Internet]. 2004 Oct [cited 2023 Apr 26];2(10). Available from:
710 https://pubmed.ncbi.nlm.nih.gov/15361934/

711 19. Statzer C, Jongsma E, Liu SX, Dakhovnik A, Wandrey F, Mozharovskyi P, et al. Youthful and age-
712 related matreotypes predict drugs promoting longevity. Aging Cell. 2021 Sep;20(9):e13441.

713 20. Ewald CY, Landis JN, Abate JP, Murphy CT, Blackwell TK. Dauer-independent insulin/IGF-1-
714 signalling implicates collagen remodelling in longevity. Nature [Internet]. 2015 Mar 3 [cited 2023
715 Feb 24];519(7541):97. Available from: /pmc/articles/PMC4352135/

716 21. Moore BT, Jordan JM, Baugh LR. WormSizer: High-throughput Analysis of Nematode Size and
717 Shape. PLoS One [Internet]. 2013 Feb 22;8(2):e57142-. Available from:
718 https://doi.org/10.1371/journal.pone.0057142

719 22. Teuscher AC, Jongsma E, Davis MN, Statzer C, Gebauer JM, Naba A, et al. The in-silico
720 characterization of the Caenorhabditis elegans matrisome and proposal of a novel collagen
721 classification. Matrix Biol Plus. 2019 Feb;1:100001.

722 23. Ewald CY. The Matrisome during Aging and Longevity: A Systems-Level Approach toward Defining
723 Matreotypes Promoting Healthy Aging. Gerontology. 2020;66(3):266–74.

724 24. Teuscher AC, Statzer C, Pantasis S, Bordoli MR, Ewald CY. Assessing Collagen Deposition During
725 Aging in Mammalian Tissue and in Caenorhabditis elegans. In 2019. p. 169–88.

726 25. Johnstone IL. Cuticle collagen genes. Trends in Genetics. 2000 Jan;16(1):21–7.

727 26. Kage-Nakadai E, Kobuna H, Kimura M, Gengyo-Ando K, Inoue T, Arai H, et al. Two Very Long
728 Chain Fatty Acid Acyl-CoA Synthetase Genes, acs-20 and acs-22, Have Roles in the Cuticle Surface
729 Barrier in Caenorhabditis elegans. PLoS One [Internet]. 2010 Jan 25 [cited 2023 Feb
730 24];5(1):e8857. Available from:
731 https://journals.plos.org/plosone/article?id=10.1371/journal.pone.0008857

732 27. Kurban G, Duplan E, Ramlal N, Hudon V, Sado Y, Ninomiya Y, et al. Collagen matrix assembly is
733 driven by the interaction of von Hippel–Lindau tumor suppressor protein with hydroxylated
734 collagen IV alpha 2. Oncogene. 2008 Feb 7;27(7):1004–12.

735 28. Sandhu A, Badal D, Sheokand R, Tyagi S, Singh V. Specific collagens maintain the cuticle
736 permeability barrier in Caenorhabditis elegans. Genetics [Internet]. 2021 Mar 31 [cited 2023 Feb
737 25];217(3). Available from: https://academic.oup.com/genetics/article/217/3/iyaa047/6123747

738 29. Zuo L, Kuo WT, Turner JR. Tight Junctions as Targets and Effectors of Mucosal Immune
739 Homeostasis. Cell Mol Gastroenterol Hepatol. 2020;10(2):327–40.

740 30. Kim MR, Cho SY, Lee HJ, Kim JY, Nguyen UTT, Ha NM, et al. Schisandrin C improves leaky gut
741 conditions in intestinal cell monolayer, organoid, and nematode models by increasing tight
742 junction protein expression. Phytomedicine. 2022 Aug;103:154209.

743 31. Muriel JM, Brannan M, Taylor K, Johnstone IL, Lithgow GJ, Tuckwell D. M142.2 (cut-6), a novel
744 Caenorhabditis elegans matrix gene important for dauer body shape. Dev Biol. 2003 Aug
745 15;260(2):339–51.

746 32. Myllyharju J. Collagens, modifying enzymes and their mutations in humans, flies and worms.
747 Trends in Genetics. 2004 Jan;20(1):33–43.

748 33. Yong R, Searcy DG. Sulfide oxidation coupled to ATP synthesis in chicken liver mitochondria.
749 Comparative Biochemistry and Physiology - B Biochemistry and Molecular Biology [Internet].

750 2001 [cited 2023 Feb 26];129(1):129–37. Available from:
751 https://pubmed.ncbi.nlm.nih.gov/11337256/

752 34. Marutani E, Morita M, Hirai S, Kai S, Grange RMH, Miyazaki Y, et al. Sulfide catabolism
753 ameliorates hypoxic brain injury. Nat Commun [Internet]. 2021 Dec 1 [cited 2023 Feb 26];12(1).
754 Available from: https://pubmed.ncbi.nlm.nih.gov/34035265/

755 35. Budde MW, Roth MB. Hydrogen sulfide increases hypoxia-inducible factor-1 activity
756 independently of von Hippel-Lindau tumor suppressor-1 in C. elegans. Mol Biol Cell [Internet].
757 2010 Jan 1 [cited 2023 Feb 26];21(1):212–7. Available from:
758 https://www.molbiolcell.org/doi/10.1091/mbc.e09-03-0199

759 36. Miller DL, Budde MW, Roth MB. HIF-1 and SKN-1 coordinate the transcriptional response to
760 hydrogen sulfide in Caenorhabditis elegans. PLoS One [Internet]. 2011 Sep 29 [cited 2023 Feb
761 26];6(9). Available from: https://pubmed.ncbi.nlm.nih.gov/21980473/

762 37. Zhao X, Zhang LK, Zhang CY, Zeng XJ, Yan H, Jin HF, et al. Regulatory effect of hydrogen sulfide on
763 vascular collagen content in spontaneously hypertensive rats. Hypertens Res [Internet]. 2008
764 [cited 2023 Feb 26];31(8):1619–30. Available from: https://pubmed.ncbi.nlm.nih.gov/18971538/

765 38. John ASP, Kundu S, Pushpakumar S, Fordham M, Weber G, Mukhopadhyay M, et al. GYY4137, a
766 Hydrogen Sulfide Donor Modulates miR194-Dependent Collagen Realignment in Diabetic Kidney.
767 Scientific Reports 2017 7:1 [Internet]. 2017 Sep 7 [cited 2023 Feb 26];7(1):1–20. Available from:
768 https://www.nature.com/articles/s41598-017-11256-3

769 39. Guan R, Wang J, Cai Z, Li Z, Wang L, Li Y, et al. Hydrogen sulfide attenuates cigarette smoke-
770 induced airway remodeling by upregulating SIRT1 signaling pathway. Redox Biol. 2020 Jan
771 1;28:101356.

772 40. Chen Y, Yuan S, Cao Y, Kong G, Jiang F, Li Y, et al. Gasotransmitters: Potential Therapeutic
773 Molecules of Fibrotic Diseases. Oxid Med Cell Longev. 2021;2021.

774 41. Sonke E, Verrydt M, Postenka CO, Pardhan S, Willie CJ, Mazzola CR, et al. Inhibition of
775 endogenous hydrogen sulfide production in clear-cell renal cell carcinoma cell lines and
776 xenografts restricts their growth, survival and angiogenic potential. Nitric Oxide [Internet]. 2015
777 Jun 26 [cited 2023 May 3];49:26–39. Available from:
778 https://pubmed.ncbi.nlm.nih.gov/26068241/

779 42. Marutani E, Morita M, Hirai S, Kai S, Grange RMH, Miyazaki Y, et al. Sulfide catabolism
780 ameliorates hypoxic brain injury. Nature Communications 2021 12:1 [Internet]. 2021 May 25
781 [cited 2023 May 3];12(1):1–19. Available from: https://www.nature.com/articles/s41467-021-
782 23363-x

783 43. Huang Y, Wang G, Zhou Z, Tang Z, Zhang N, Zhu X, et al. Endogenous Hydrogen Sulfide Is an
784 Important Factor in Maintaining Arterial Oxygen Saturation. Front Pharmacol. 2021 May
785 31;12:1366.

786 44. Forgan LG, McNeill BA, DeLeon E, Gao Y, Olson K. Effects of Hypoxia on Hydrogen Sulfide
787 Production and Degradation Gene Expression Pathways. The FASEB Journal [Internet]. [cited
788 2023 May 3];31:700.9-700.9. Available from:
789 https://onlinelibrary.wiley.com/doi/full/10.1096/fasebj.31.1_supplement.700.9

790 45. Uba T, Matsuo Y, Sumi C, Shoji T, Nishi K, Kusunoki M, et al. Polysulfide inhibits hypoxia-elicited
791 hypoxia-inducible factor activation in a mitochondria-dependent manner. Mitochondrion. 2021
792 Jul 1;59:255–66.

793 46. Budde MW, Roth MB. Hydrogen sulfide increases hypoxia-inducible factor-1 activity
794 independently of von Hippel-Lindau tumor suppressor-1 in C. elegans. Mol Biol Cell. 2010 Jan
795 1;21(1):212–7.

796 47. Wu B, Teng H, Zhang L, Li H, Li J, Wang L, et al. Interaction of Hydrogen Sulfide with Oxygen
797 Sensing under Hypoxia. Oxid Med Cell Longev [Internet]. 2015 [cited 2023 May 3];2015. Available
798 from: https://pubmed.ncbi.nlm.nih.gov/26078818/

799 48. Ellmers L, Templeton E, … APIJ of, 2020 undefined. Hydrogen sulfide treatment improves post-
800 infarct remodeling and long-term cardiac function in CSE knockout and wild-type mice. mdpi.com
801 [Internet]. [cited 2023 May 3]; Available from: https://www.mdpi.com/744314

802 49. Teuscher AC, Jongsma E, Davis MN, Statzer C, Gebauer JM, Naba A, et al. The in-silico
803 characterization of the Caenorhabditis elegans matrisome and proposal of a novel collagen
804 classification. Matrix Biol Plus. 2019 Feb;1:100001.

805 50. Choe KP, Strange K. Genome-wide RNAi screen and in vivo protein aggregation reporters identify
806 degradation of damaged proteins as an essential hypertonic stress response. Am J Physiol Cell
807 Physiol [Internet]. 2008 Dec [cited 2023 Feb 27];295(6):1488–98. Available from: www.ajpcell.org

808 51. Hine C, Harputlugil E, Zhang Y, Ruckenstuhl C, Lee BC, Brace L, et al. Endogenous hydrogen sulfide
809 production is essential for dietary restriction benefits. Cell [Internet]. 2015 Jan 15 [cited 2023 Feb
810 27];160(1–2):132–44. Available from: https://pubmed.ncbi.nlm.nih.gov/25542313/

811 52. Qabazard B, Ahmed S, Li N, Arlt VM, Moore PK, Stürzenbaum SR. C. elegans aging is modulated
812 by hydrogen sulfide and the sulfhydrylase/cysteine synthase cysl-2. PLoS One. 2013 Nov 8;8(11).

813 53. Qabazard B, Li L, Gruber J, Peh MT, Ng LF, Kumar SD, et al. Hydrogen sulfide is an endogenous
814 regulator of aging in Caenorhabditis elegans. Antioxid Redox Signal [Internet]. 2014 Jun 1 [cited
815 2023 Feb 27];20(16):2621–30. Available from: https://pubmed.ncbi.nlm.nih.gov/24093496/

816 54. Ng LT, Ng LF, Tang RMY, Barardo D, Halliwell B, Moore PK, et al. Lifespan and healthspan benefits
817 of exogenous H2S in C. elegans are independent from effects downstream of eat-2 mutation. npj
818 Aging and Mechanisms of Disease 2020 6:1 [Internet]. 2020 Jun 10 [cited 2023 Feb 27];6(1):1–14.
819 Available from: https://www.nature.com/articles/s41514-020-0044-8

820 55. Lohakul J, Jeayeng S, Chaiprasongsuk A, Torregrossa R, Wood ME, Saelim M, et al. Mitochondria-
821 Targeted Hydrogen Sulfide Delivery Molecules Protect Against UVA-Induced Photoaging in
822 Human Dermal Fibroblasts, and in Mouse Skin In Vivo. Antioxid Redox Signal [Internet]. 2022 Jun
823 1 [cited 2023 Apr 30];36(16–18):1268–88. Available from:
824 https://pubmed.ncbi.nlm.nih.gov/34235951/

825 56. Rahimi M, Sohrabi S, Murphy CT. Novel elasticity measurements reveal C. elegans cuticle stiffens
826 with age and in a long-lived mutant. Biophys J. 2022 Feb 15;121(4):515–24.

827 57. Pu YZ, Wan QL, Ding AJ, Luo HR, Wu GS. Quantitative proteomics analysis of Caenorhabditis
828 elegans upon germ cell loss. J Proteomics. 2017 Mar 6;156:85–93.

829 58. Wei Y, Kenyon C. Roles for ROS and hydrogen sulfide in the longevity response to germline loss in
830 Caenorhabditis elegans. Proc Natl Acad Sci U S A [Internet]. 2016 May 17 [cited 2023 Feb
831 27];113(20):E2832–41. Available from:
832 https://www.pnas.org/doi/abs/10.1073/pnas.1524727113

833 59. Bolger AM, Lohse M, Usadel B. Trimmomatic: a flexible trimmer for Illumina sequence data.
834 Bioinformatics. 2014 Aug 1;30(15):2114–20.

835 60. Dobin A, Davis CA, Schlesinger F, Drenkow J, Zaleski C, Jha S, et al. STAR: ultrafast universal RNA-
836 seq aligner. Bioinformatics. 2013 Jan 1;29(1):15–21.

837 61. Anders S, Huber W. Differential expression analysis for sequence count data. Genome Biol. 2010
838 Oct 27;11(10):R106.

839 62. Love MI, Huber W, Anders S. Moderated estimation of fold change and dispersion for RNA-seq
840 data with DESeq2. Genome Biol. 2014 Dec 5;15(12):550.

841 63. Ritchie ME, Phipson B, Wu D, Hu Y, Law CW, Shi W, et al. limma powers differential expression
842 analyses for RNA-sequencing and microarray studies. Nucleic Acids Res. 2015 Apr 20;43(7):e47.

843 64. Adrian Alexa and Jörg Rahnenführer. topGO: Enrichment Analysis for Gene Ontology. R package
844 version 2.46.0. 2021. topGO: Enrichment Analysis for Gene Ontology. R package version 2.46.0.

845 65. Alexa A, Rahnenführer J, Lengauer T. Improved scoring of functional groups from gene expression
846 data by decorrelating GO graph structure. Bioinformatics. 2006 Jul 1;22(13):1600–7.

847 66. Raivo Kolde. https://CRAN.R-project.org/package=pheatmap. 2019. pheatmap: Pretty Heatmaps.
848 R package version 1.0.12.

67. Kage-Nakadai E, Kobuna H, Kimura M, Gengyo-Ando K, Inoue T, Arai H, et al. Two very long chain fatty acid acyl-CoA synthetase genes, acs-20 and acs-22, have roles in the cuticle surface barrier in Caenorhabditis elegans. PLoS One. 2010 Jan 25;5(1):e8857.

68. Rieckher M, Tavernarakis N. Caenorhabditis elegans Microinjection. Bio Protoc. 2017;

69. Stroustrup N, Ulmschneider BE, Nash ZM, López-Moyado IF, Apfeld J, Fontana W. The Caenorhabditis elegans Lifespan Machine. Nat Methods. 2013 Jul 12;10(7):665–70.

878 ## Supporting information captions

879

880 **Suppl. Figure 1: Regulation of genes associated with common ECM related phenotypes**

881 Expression change of genes associated with the dumpy phenotype compared to WT; **B)** Respective analysis for genes
882 associated with the long phenotype; **C)** Respective analysis for genes associated with the roller phenotype; **D)** Number
883 of dauer animals measured by % of survival after treatment with SDS after normal culture (20°C) or dauer inducing
884 culture (starving at 25°C). The group of genes associated with each phenotype was taken from the Matrisome project
885 (22). Boxes and whiskers represent the 25-75th percentile and the minimum to maximum values, respectively.
886 Significance was calculated by comparing the mean value each group with a One-Way ANOVA followed by a Tukey
887 post-hoc. * indicates a $p<0.05$ for the comparison in between the signaled groups.

888

889 **Suppl. Figure 2: Collagen reporter expression, stress resistance, and cuticle associated reporters**

890 Representative images of the blotting against GFP in *col-19*::GFP WT and *vhl-1(ok161)* backgrounds; **B)** Densiometry
891 measurements of A**; C)** Survival curve of animals exposed to paraquat 10mM**; D)** Representative pictures of the MUP-
892 4::GFP reporter**; E)** Representative pictures of the AJM-1::GFP reporter; **F)** Representative pictures of the SCM::GFP
893 reporter. Significance was calculated by comparing the mean value each group with a T-student test or a survival
894 Keplan-Meier analysis. *** indicates a $p<0.001$ for the comparison in between the signaled groups.

895

896 **Suppl. Figure 3: Tissue-specific rescue of *vhl-1*::GFP expression and RNAi screen for size regulators**

897 **A)** Representative pictures of L1 worms expressing *pvhl-1::vhl-1*::GFP; **B)** Size of *vhl-1(ok161)* worms expressing *vhl-*
898 *1::*GFP in the intestine driven by the *elt-2* promoter; **C)** Size of *vhl-1(ok161)* worms expressing *vhl-1::*GFP in the neurons
899 driven by the unc-*119* promoter; **D))** Size of *vhl-1(ok161)* worms expressing *vhl-1::*GFP in the cuticle driven by the *dpy-*
900 *7* promoter; **E)** Size of *vhl-1(ok161)* F1 worms of which P0 was exposed to RNAi against the indicated genes, including
901 *sqrd-1* in red. Significance was calculated by comparing the mean value each group with a One-Way ANOVA followed
902 by a Tukey post-hoc or t-test Student when only two groups were present. * indicates a $p<0.05$ for the comparison of
903 any group with vhl-1(ok161) alone or in empty vector (EV) RNAi.

904

905 **Suppl. Figure 4: Expression of different collagen candidates**

906 Expression of *col-17, col-63, col-78*, and *col-88, and col-156* in *vhl-1(ok161)*, *sqrd-1(ar13)*, and *sqrd-1/vhl-1* double
907 mutant. mRNA amounts is expressed as fold change compared to the WT expression levels (dotted line) of each

908 respective collagen. Significance was calculated by comparing the mean value each group with an One-Way ANOVA
909 followed by a Tukey post-hoc.
910
911 **Suppl. Table 1: RNAseq data from *vhl-1(ok161)*, *hif-1(ia4)*, and *vhl-1;hif-1* double mutant.**
912 Values are expressed as fold change (log2), whereas green values signal significant upregulation, red signals
913 significant downregulation, and white values signal no change compared to *WT* controls. Statistically significant
914 differences between WT and the other groups was calculated the R package DeSeq2.
915
916 **Suppl. Table 2: RNAseq data regarding the top regulated collagen genes in *vhl-1(ok161)* mutants:**
917 Values are expressed as fold change (log2), whereas green values signal significant upregulation, red signals
918 significant downregulation for the described comparison. Statistically significant differences between WT and the other
919 groups was calculated calculated the R package DeSeq2.
920
921
922

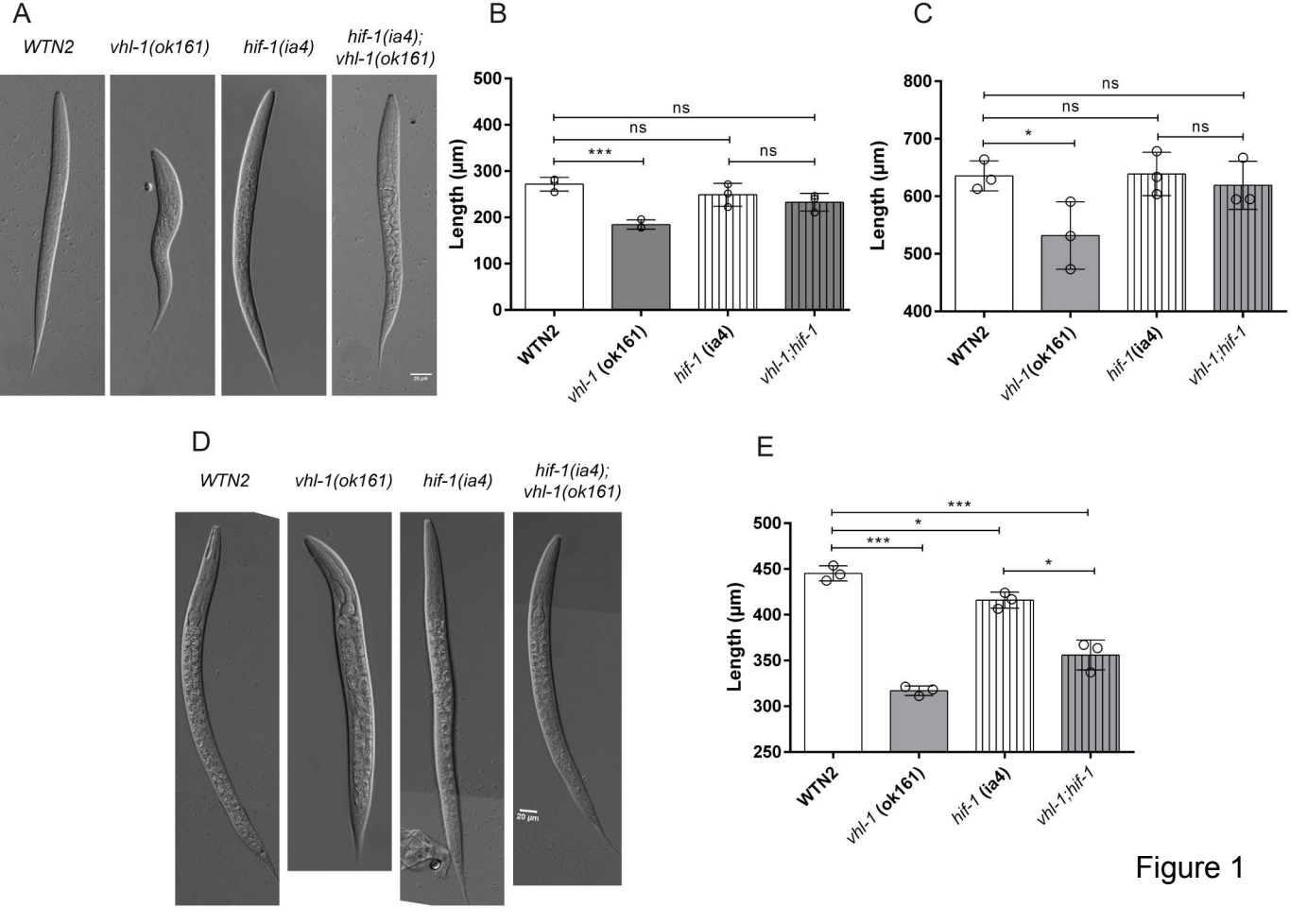
A
WTN2
vhl-1(ok161)
hif-1(ia4)
hif-1(ia4);
vhl-1(ok161)
B
Length (µm)
500
400
300
200
100
0
ns
ns
***
ns
WTN2
vhl-1 (ok161)
hif-1 (ia4)
vhl-1;hif-1
C
Length (µm)
800
700
600
500
400
ns
ns
*
ns
WTN2
vhl-1(ok161)
hif-1(ia4)
vhl-1;hif-1
D
WTN2
vhl-1(ok161)
hif-1(ia4)
hif-1(ia4);
vhl-1(ok161)
20 µm
E
Length (µm)
500
450
400
350
300
250
***
*
***
*
WTN2
vhl-1 (ok161)
hif-1 (ia4)
vhl-1;hif-1

Figure 1

Figure 2

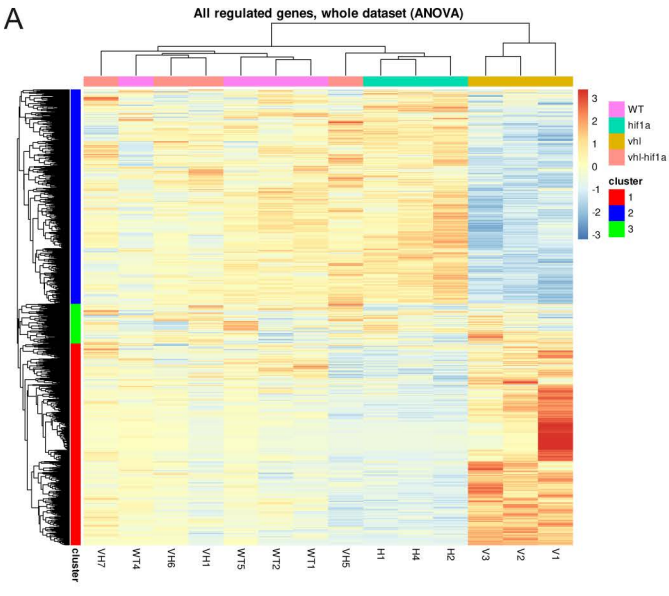
A
All regulated genes, whole dataset (ANOVA)
WT
hif1a
vhl
vhl-hif1a
cluster
1
2
3
VH7
WT4
VH6
VH1
WT5
WT2
WT1
VH5
H1
H4
H2
V3
V2
V1

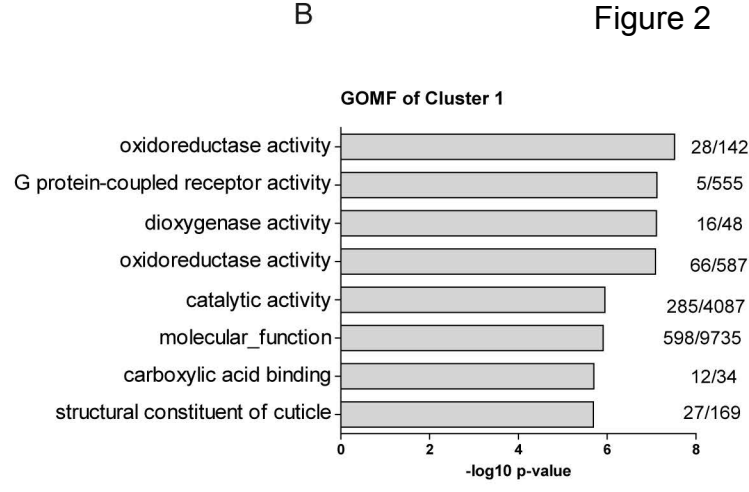
B
GOMF of Cluster 1
oxidoreductase activity 28/142
G protein-coupled receptor activity 5/555
dioxygenase activity 16/48
oxidoreductase activity 66/587
catalytic activity 285/4087
molecular_function 598/9735
carboxylic acid binding 12/34
structural constituent of cuticle 27/169
-log10 p-value

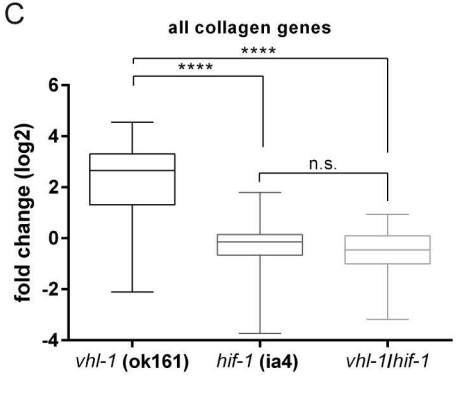
C
all collagen genes
fold change (log2)
****
****
n.s.
vhl-1 (ok161)
hif-1 (ia4)
vhl-1/hif-1

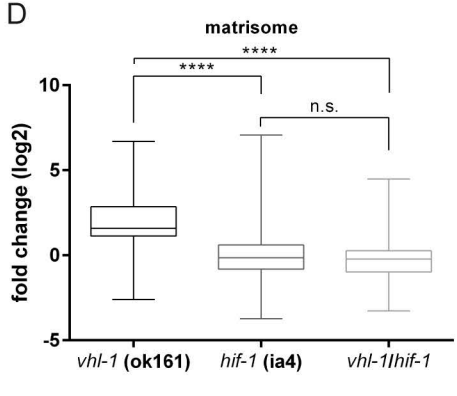
D
matrisome
fold change (log2)
****
****
n.s.
vhl-1 (ok161)
hif-1 (ia4)
vhl-1/hif-1

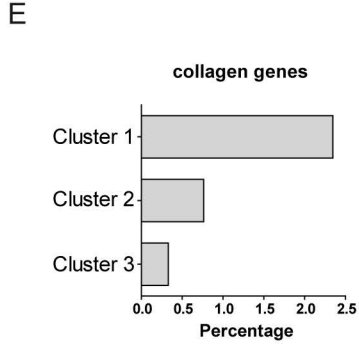
E
collagen genes
Cluster 1
Cluster 2
Cluster 3
Percentage

Figure 3

A

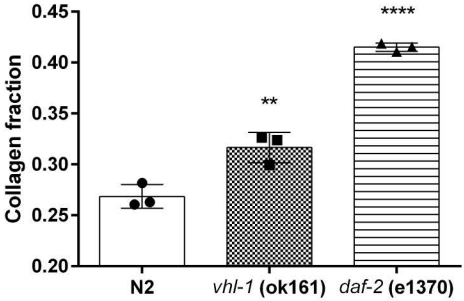

B

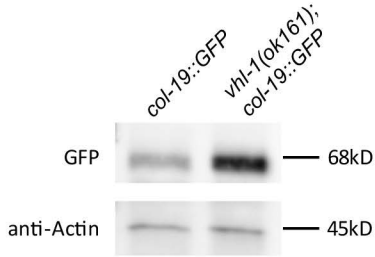

C

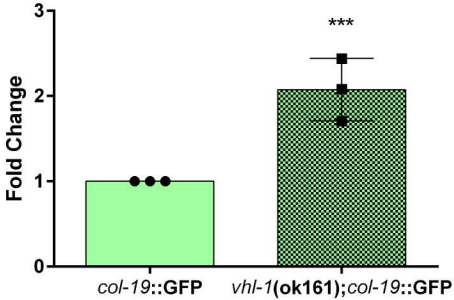

D

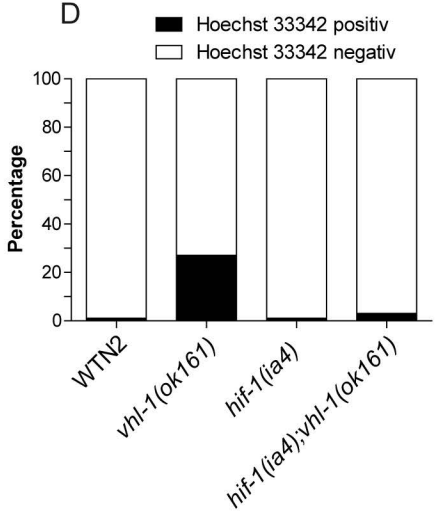

E

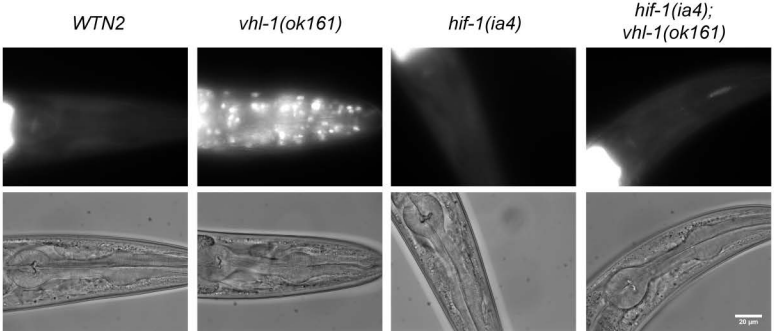

Figure 4

A

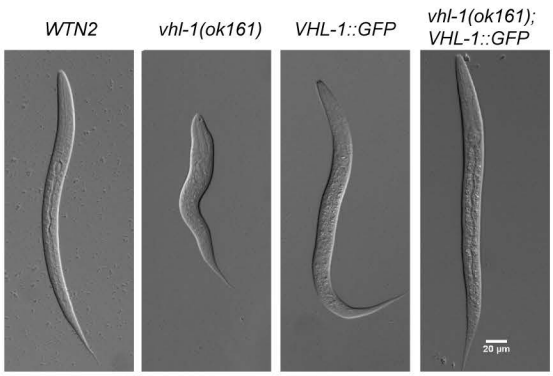

B

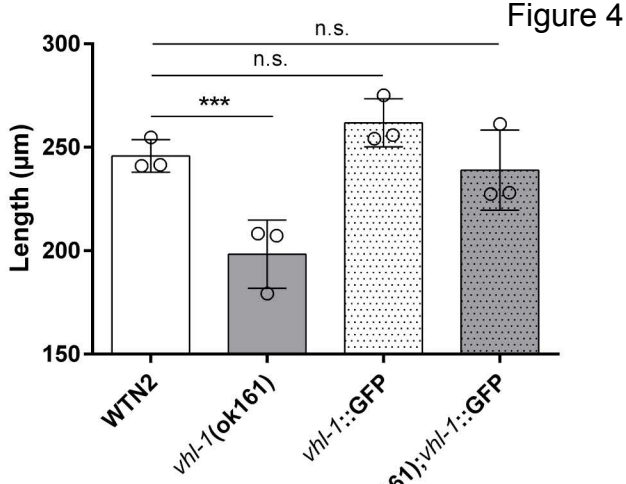

C

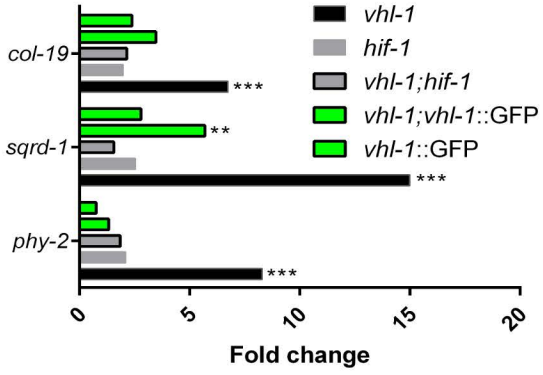

D

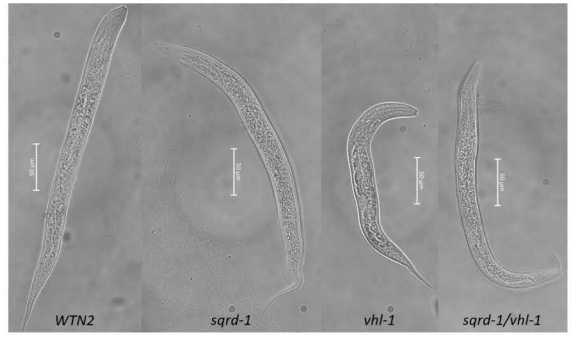

E

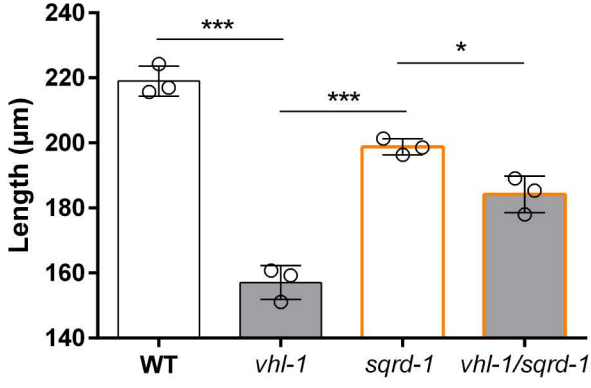

F

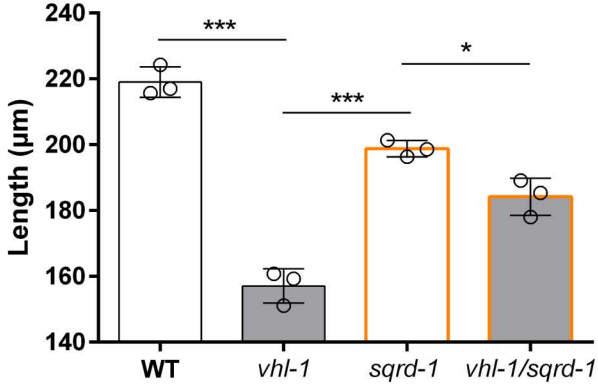

Figure 5

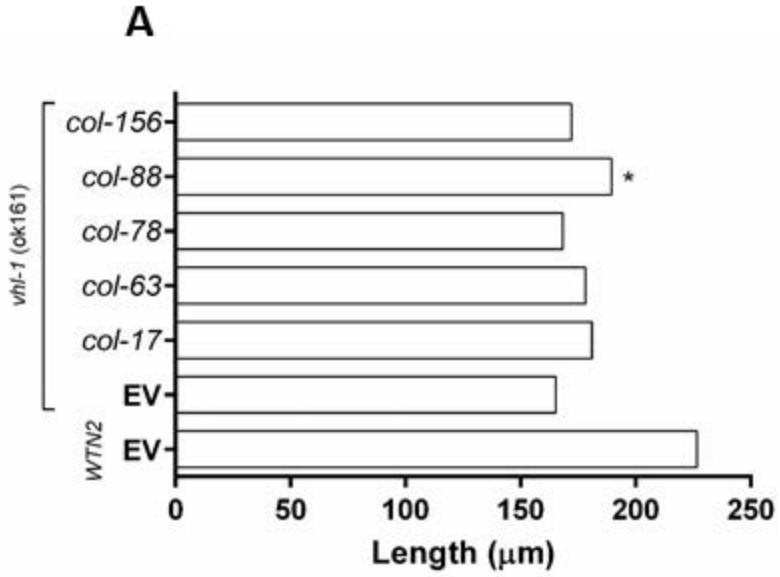
A
col-156
col-88
col-78
col-63
col-17
EV
EV
vhl-1 (ok161)
WTN2
*
0
50
100
150
200
250
Length (µm)

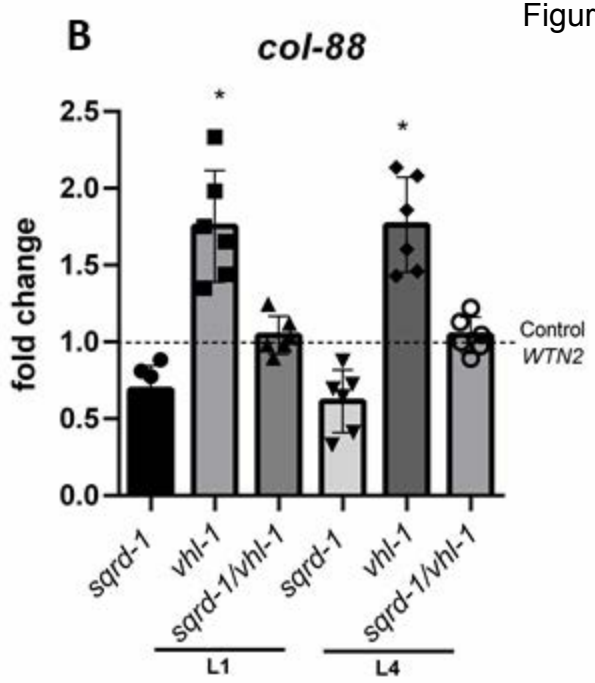
B
col-88
fold change
2.5
2.0
1.5
1.0
0.5
0.0
*
*
Control
WTN2
sqrd-1
vhl-1
sqrd-1/vhl-1
sqrd-1
vhl-1
sqrd-1/vhl-1
L1
L4

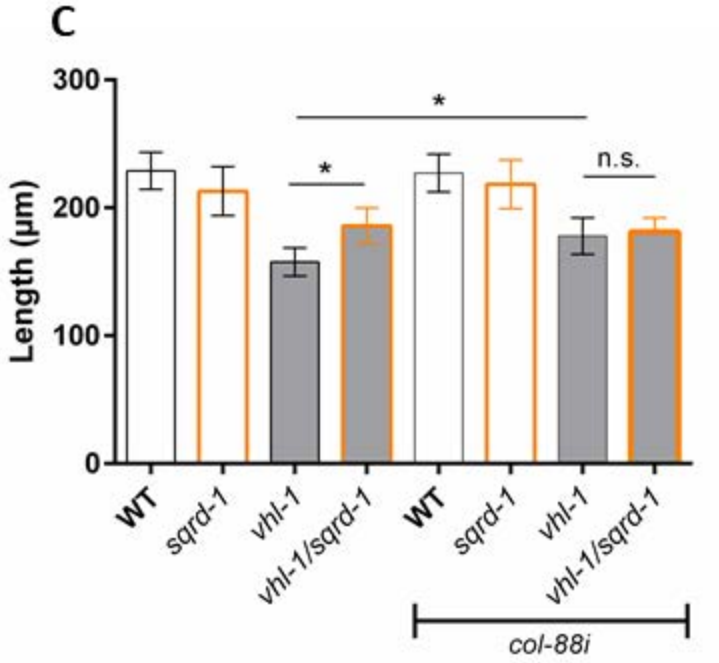
C
Length (µm)
300
200
100
0
*
*
n.s.
WT
sqrd-1
vhl-1
vhl-1/sqrd-1
WT
sqrd-1
vhl-1
vhl-1/sqrd-1
col-88i

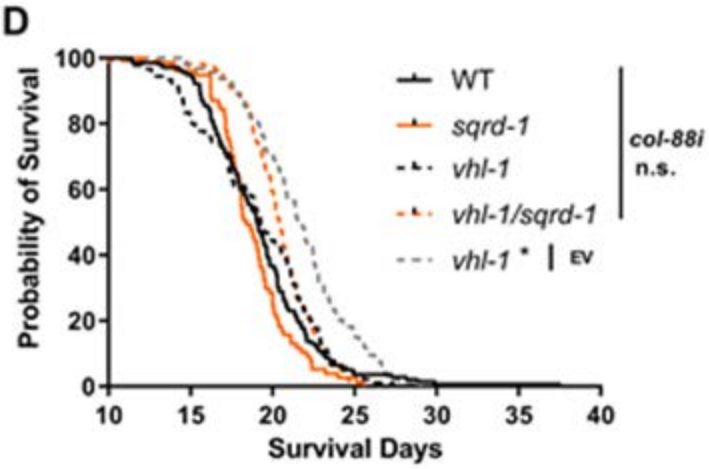
D
Probability of Survival
100
80
60
40
20
0
10
15
20
25
30
35
40
Survival Days
WT
sqrd-1
vhl-1
vhl-1/sqrd-1
vhl-1 *
EV
col-88i
n.s.